Calderon, V. H., and Baker, J. W. (2026). "Observed Ground Motions That Exceeded Design Response Spectra in the Western United States." *Earthquake Spectra*, 42(1), e70040. https://doi.org/10.1002/esp4.70040

Observed ground motions that exceeded design response spectra in the Western United States

Victor H. Calderon, M.EERI[1] and Jack W. Baker, M.EERI[1]

Abstract

Seismic design values are intended to be rarely exceeded, yet their reasonableness is often debated. This paper uses ground motion recordings to document exceedances of four contemporary seismic design spectra in the Western U.S.: the risk-targeted maximum considered earthquake (MCE_R) spectrum, its probabilistic component without the deterministic cap, and the design earthquake spectrum (all from ASCE/SEI 7-22), as well as the 2475-year uniform-hazard spectrum from the 2023 USGS National Seismic Hazard Model. We compare each recording's RotD100 spectral acceleration to its site-specific target spectra and interpret the results through seismic hazard disaggregation at selected locations. The survey reveals that all target spectra are exceeded by multiple recordings. MCE_R exceedances concentrate near active California faults at short source-to-site distances and short periods, primarily driven by moderate-magnitude events, with the deterministic cap increasing exceedance rates relative to the underlying probabilistic spectrum. Long-period exceedances ($T > 1$ s), caused by infrequent large-magnitude earthquakes, are relatively sparse. Frequent short-distance and small-magnitude exceedances explain the observed high total residuals compared to disaggregation-based epsilons. These observations demonstrate that high-amplitude code spectra are physically attainable and encourage shifting the debate from the spectra's reasonableness toward balancing safety and construction costs.

Keywords

Seismic hazard, ground motion, seismic design spectrum, ASCE 7, USGS National Seismic Hazard Model

[1]Stanford University, Stanford, CA, USA

Corresponding author:
Victor Calderon, Stanford University, 473 Via Ortega, Stanford, CA 94305, USA
Email: vcalast@alumni.stanford.edu

Prepared using sagej.cls *[Version: 2017/01/17 v1.20]*

Introduction

Modern national seismic design value maps rely heavily on results from probabilistic seismic hazard analysis (PSHA). Design ground motion amplitudes are selected based on a target frequency of exceedance or based on a value that ensures a limited level of collapse risk when the accompanying design procedures are utilized (Luco et al., 2007; Stewart et al., 2020). These criteria can lead to very large ground motion amplitudes close to active faults. Therefore, some design procedures place deterministic limits, or "caps" on amplitudes in such circumstances. Much of the deliberation about code spectra targets is not documented in writing, but the claim that probabilistic amplitudes can produce "overly conservative or impractical" design loads is an example of the opinions held by some (Hamburger et al., 2017).

Probabilistic, risk-targeted, or deterministic resulting design ground motion values are, by definition, rare and thus difficult to validate empirically. However, given the importance of validation, many approaches have been attempted to compare hazard analyses with observed ground shaking. Basic PSHA produces forecasts of ground motion intensity level exceedances (i.e., hazard curves) for a wide range of rates, hence validation tests can tally observed exceedances and compare them with hazard forecasts (e.g. Stirling and Petersen, 2006; Beauval et al., 2008; Gerstenberger et al., 2020; Mak and Schorlemmer, 2016). Such tests naturally focus on frequently-exceeded low-amplitude shaking that is more readily quantifiable from observations. Seismic hazard analyses have also been compared to observations that provide proxies for shaking amplitude, but are available over larger spatial or temporal domains than ground motion recordings. Hazard curves have been compared to felt shaking intensities (e.g. Brooks et al., 2018; Salditch et al., 2024), or to evidence of strong shaking from fragile geologic features (e.g. Brune, 1996). While such methods are more useful for validating predictions of rare shaking, they are also more complex and have not been utilized in the context of evaluating code spectra.

The interpretation of the exceedances of the PSHA-based hazard levels have been the subject of extensive discussion over the past two decades (e.g., Bommer and Abrahamson, 2006; Iervolino, 2022; Bradley, 2025). Much of this discussion has been around whether exceedances or changes in the hazard level estimates reflect deficiencies in underlying models, the epistemic uncertainty in rare earthquake event predictions, or how PSHA products are used for engineering purposes (Douglas et al., 2024). These discussions have been particularly active in regions where updates to the national hazard models lead to noticeable changes in the seismic design value maps, raising questions about the practical implications of such differences (Hamburger et al., 2017; Petersen et al., 2021).

In this study, we compare observed ground motions with the contemporary seismic design levels in the Western United States. Specifically, we focus on the ASCE/SEI 7-22 (ASCE, 2021) design earthquake (DE) and risk-targeted maximum considered earthquake spectra (MCE_R), both based on the 2018 U.S. Geological Survey (USGS) National Seismic Hazard Model (NSHM), and on the uniform hazard spectra with a 2475-year return period from the recent 2023 USGS NSHM. Only exceedances of these

high-amplitude spectra are considered, given their direct relevance to design practice and the frequent debate regarding their reasonableness. Rather than attempt to validate predicted exceedance rates, here we only document the number, geographic distribution, and circumstances associated with observed exceedances.

In this sense, we examine the features of the earthquakes, ground motions, and design spectra associated with exceedances. The analysis is restricted to ground motion recordings in the conterminous Western U.S., where the high seismic hazard, widespread use of deterministic limits, and the availability of high-quality ground motion data provide a test bed for future revisions to seismic design values.

Methods and Data

Recorded Ground Motion Data

We utilize the NGA-West2 database of 21,540 recorded ground motions from shallow active crustal earthquakes (Ancheta et al., 2014). This database includes recordings from the Western U.S. (including Alaska) and a number of international recordings. We excluded all non-U.S. recordings and restricted the dataset to the conterminous Western U.S. Although Alaska recordings were included in an initial screening, none exceeded the target spectra, so they were not considered further. We removed recordings with missing average shear wave velocity to a depth of 30 m (V_{S30}) values, with $V_{S30} < 150$ m/s, with unknown geographic locations, or missing spectral acceleration (SA) values.

This selection process resulted in 15,111 records being available for the analysis. The dataset encompasses events with magnitudes ranging from 2.99 to 7.4 at closest distances to the rupture (R_{rup}) ranging from 0.07 to 779.6 km, with V_{S30} varying from 155 to 1464 m/s. For each recording, we consider the maximum spectral response acceleration in all horizontal orientations ($SA_{RotD100}$), at 105 periods ranging from 0.01 to 10 seconds.

Record processing restricts the ground motion recordings' ranges of usable frequencies. Figure 1 shows the number of usable ground motions as a function of the period, for all considered recordings as well as subsets of larger-magnitude recordings. While there are many fewer usable ground motions at periods of five to 10 seconds, the large majority of motions are usable to periods of up to two seconds.

Target Spectra

We compare the ground motion recordings to four target spectra, each calculated at the location of the seismic record using the preferred V_{S30} value from the NGA-West2 database. These values are selected from a set of methods that infer V_{S30} from available measurements, with expert judgment determining the preferred value for each site (Ancheta et al., 2014). All target spectra are computed for $SA_{RotD100}$ response to ensure consistency when comparing to the recordings' $SA_{RotD100}$ values.

The first target is the multi-period, risk-targeted maximum considered earthquake (MCE_R) response spectrum from ASCE 7-22 (2021). The site class is determined by classifying the NGA-West2 preferred V_{S30} according to ASCE 7-22. This spectrum is composed of both probabilistic and deterministic elements. The "probabilistic MCE_R"

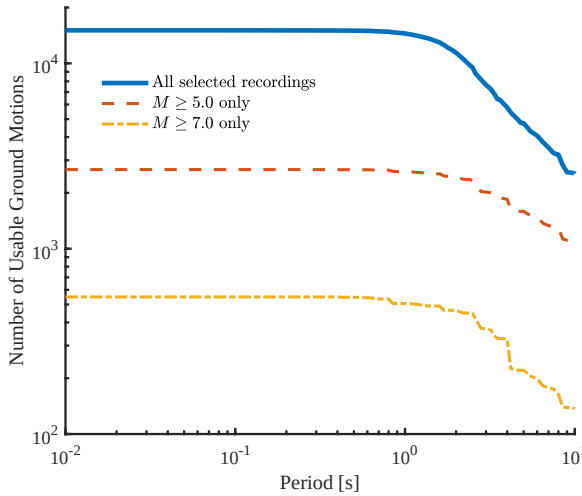

Figure 1. Number of usable ground motions as a function of the spectral acceleration period of vibration.

is obtained by combining a hazard curve and a fragility function to find a spectral acceleration that is expected to achieve a 1% probability of structural collapse in 50 years (see Chapter 21 of ASCE, 2021). For most locations within the study area, the probabilistic MCE_R is the MCE_R.

The deterministic MCE_R is also computed, as the largest 84th percentile ground motion level associated with any known nearby fault (i.e., a 16% chance of being exceeded, given the occurrence of a large earthquake on the fault). The deterministic MCE_R can be used as the MCE_R if it is less than the probabilistic MCE_R, as long as it exceeds a lower-limit threshold. For each site class, this lower limit is defined in the ASCE 7 as the 84th-percentile ground motion level for an M 8.0 shallow crustal earthquake at 12.5 km from the fault rupture. Figure 2 illustrates this calculation. This reduction to the deterministic MCE_R is often referred to as a "deterministic cap," and it only occurs near faults.

Given the significant influence of the deterministic cap on the analyses presented below, the second target spectrum is the probabilistic MCE_R alone (i.e., the MCE_R without applying the deterministic cap). The probabilistic MCE_R response spectrum is also shown in Figure 2.

The third target is the design earthquake (DE) response spectrum. It is computed as two-thirds of the MCE_R spectral accelerations (see Chapter 11 of ASCE, 2021). This spectrum is used in some seismic design procedures in the code, so its exceedance is also of interest. It is lower in amplitude than the other targets, and so is exceeded more frequently.

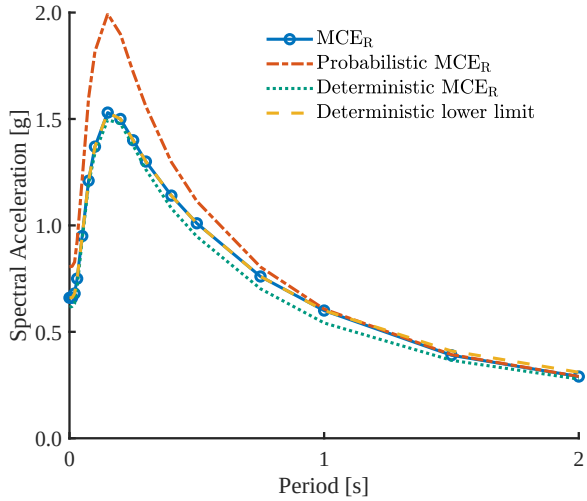

Figure 2. Illustration of the components of the multi-period, risk-targeted maximum considered earthquake (MCE_R) response spectrum for the Pinon Flats Observatory station.

The fourth target is the uniform hazard spectrum (UHS), calculated for a 2% probability of exceedance in 50 years (i.e., a return period, or RP, of 2,475 years). This spectrum is obtained from the 2023 USGS National Seismic Hazard Model (Petersen et al., 2024). This spectrum is often similar in amplitude to the probabilistic MCE_R. Use of this spectrum allows us to consider the newly released 2023 USGS NSHM, which does not yet have formal associated MCE_R values for the ASCE 7-22 standard.

To understand the earthquake scenarios driving the exceedance of target spectra, we employ disaggregation of the UHS hazard results. At each vibration period T, disaggregation decomposes the aggregated hazard to identify the earthquake scenarios that contribute to exceedances (Bazzurro and Cornell, 1999; Baker et al., 2021). The results are commonly summarized by the mean magnitude ($\overline{M}$), distance ($\overline{R}_{rup}$), and epsilon ($\bar{\varepsilon}$) of the earthquake scenarios that contribute to exceeding the given target spectral amplitude. The magnitude and distance are physical source properties, and ε represents how many standard deviations the earthquake ground motion lie above ($\varepsilon > 0$) or below ($\varepsilon < 0$) the median prediction for that earthquake rupture (e.g., $\varepsilon = 0$ corresponds to the median, and $\varepsilon = 1$ is the 84th percentile amplitude).

The MCE_R and DE spectra are obtained from the ASCE Hazard Tool, whereas the probabilistic and deterministic MCE_R spectra were retrieved from the dataset provided by (Luco et al., 2021). The UHS and disaggregation products are obtained from the USGS Earthquake Hazard Toolbox (Clayton and Powers, 2023). See the Data and Resources section for more information. The target multi-period code spectra are considered here because of their greater compatibility with the shapes of real record spectra. The code spectra are also available as a 'two-period' spectrum with an idealized shape interpolated

between the two periods with specified amplitudes. Comparable analyses using the two-period spectra are provided in the Supplemental Materials.

Results and Analysis

We compare the ground motion recordings to the four corresponding target spectra to study any exceedances. Figure 3 illustrates the comparison of a single recording and its corresponding target spectra. The recording exceeds the UHS at periods from 0.14 to 0.17 s. It exceeds the probabilistic MCE_R at the same periods and also from 0.35 to 0.36 s. It exceeds the MCE_R from 0.13 to 0.2 s and 0.33 to 0.38 s. The design response spectrum is exceeded from 0 to 0.05 s, again from 0.06 to 0.07 s, and finally from 0.095 to 0.46 s.

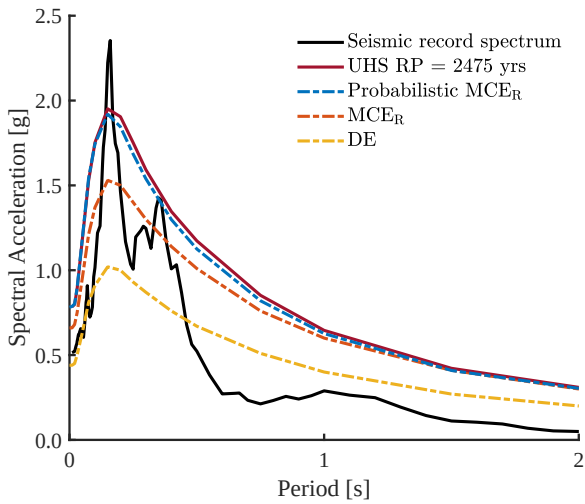

Figure 3. Comparison of the UCSC Lick Observatory recording spectrum from the 1989 Loma Prieta earthquake with the target spectra at the recording location.

Figure 4a shows the number of recordings that exceed each target spectrum at each period. There are 170 recordings exceeding the DE response spectrum, 63 exceeding the MCE_R, 42 exceeding the UHS, and 34 exceeding the probabilistic MCE_R. It is not surprising that the DE response spectra have a larger number of exceedances than the other target spectra, given that they are defined with lower spectral acceleration values than the other targets. It is notable that the number of exceedances falls off at longer periods of vibration, with the number of exceedances decreasing for $T > 0.2$ s, and being substantially reduced for $T > 1$ s. There are fewer usable recordings at long periods (Figure 1). But the drop in Figure 4a begins at shorter periods than the drop due to usable periods (visible at $T > 2$ s in Figure 1). In addition, the recordings with long-period amplitudes greater than the target spectra would likely have usable signal; otherwise such recordings would not have not been able to capture the long-period amplitudes or would

have been removed during processing, so this pattern is likely not an artifact of record processing. A figure presenting the number of exceedances in the two-period response spectra is also included in the Supplemental Materials.

Figure 4b shows the 1706 stations with a recording considered in this study, and the 163 stations with a recording that exceeded any of the target spectra. The recordings span Oregon, California, Idaho, Montana, and Nevada; however, most exceedances are concentrated along western California. By comparison, only one exceedance was identified in each of Idaho, Montana, and Nevada. For all target spectra considered, 22 or fewer stations experienced exceedances from two or more different earthquakes. For instance, the El Centro Differential Array station MCE_R spectrum is exceeded by both the 1979 Imperial Valley and the 2010 El Mayor earthquakes.

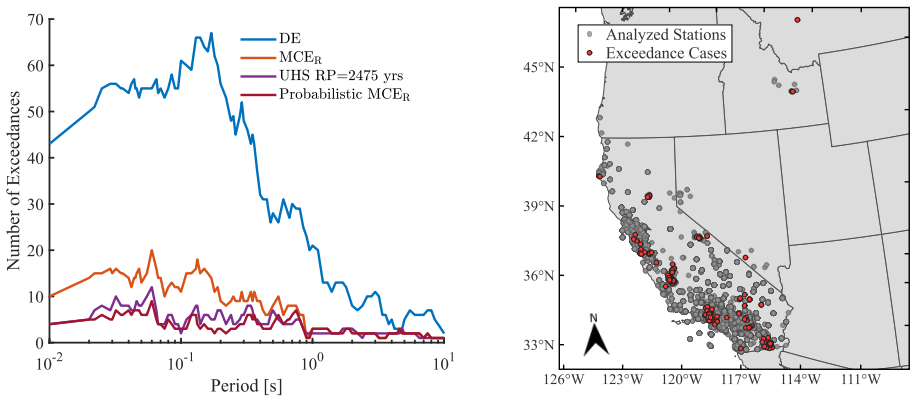

Figure 4. (a) Number of records that exceeded the target spectra at a given period. b) Map of the locations of stations with recordings considered in this study. Stations with recordings exceeding any target spectra are indicated with a separate symbol.

Figure 5 shows the magnitudes and distances of the considered recordings, noting those that exceed the MCE_R targets at short and long periods. This indicates that short-period exceedances come from a broader range of magnitudes, while long-period exceedances only come from relatively large earthquakes. At short periods, 56 recordings exceed the MCE_R spectrum, but less than half of them exceed the probabilistic MCE_R. The eight recordings that cause the long-period exceedances exceed both target spectra. In addition, all exceedances occurred at rupture distances of less than 50 km, and most occurred at less than 20 km, indicating that large ground motions at both short and long-periods occur near fault regions (Kaneko and Goto, 2022). This distance range was expected, as high-amplitude ground motions at short distances have not yet been strongly reduced by attenuation effects (Baker et al., 2021).

From a PSHA perspective, exceedance likelihood reflects a trade-off between the event occurrence rate and the conditional probability of exceeding a fixed spectral

acceleration given the event magnitude M and rupture distance R_{rup}. While small-magnitude events occur more frequently, their conditional probability of exceeding high spectral acceleration levels is generally low; in contrast, rarer events with larger magnitudes or smaller R_{rup} values have a substantially higher conditional exceedance probability. As a result, earthquake events with $R_{rup} \leq 50$ km are more likely to produce exceedances, because the conditional exceedance probability increases sharply at small distances (Iervolino et al., 2019; Minson et al., 2021).

The frequency of recordings that exceed the MCE_R targets in each range of periods can be primarily associated with the effect of the deterministic cap and the characteristics of the causal earthquake, both of which are discussed further below.

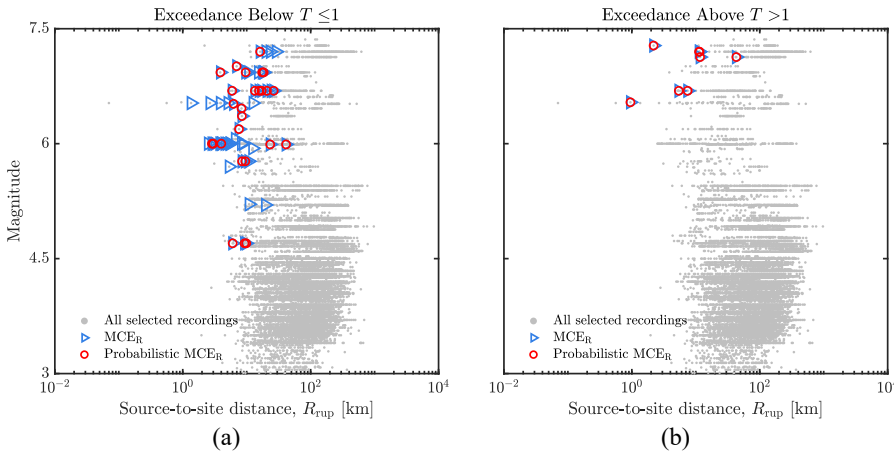

Figure 5. Magnitude$-R_{rup}$ distribution of the considered recordings, highlighting cases that exceed the MCE_R the probabilistic MCE_R. a) Recordings that exceed the targets at periods less than or equal to one second. b) Recordings that exceed the targets at periods greater than one second.

To study the effect of the deterministic cap on MCE_R exceedances, Figure 6 shows the MCE_R and probabilistic MCE_R spectra of two cases where a recording's spectrum exceeded them at short and long periods. In the regions where the deterministic cap has influence, the cap tends to significantly decrease the spectral ordinates at short periods, and therefore enlarge the range of periods where recordings exceed the target (as seen in Figure 6a). Longer periods are typically not influenced by the deterministic cap (Figure 6b).

To illustrate the localized effect of the deterministic cap, in Figure 7, we mapped the stations where the MCE_R spectrum or the probabilistic MCE_R are exceeded, along with the causal earthquakes. Many cases are in four distinct regions: 1) Santa Cruz (from the 1989 Loma Prieta earthquake); 2) Parkfield and Coalinga (2004 Parkfield and 1983 Coalinga earthquake sequence); 3) Los Angeles (mostly from the 1994 Northridge earthquake); and 4) El Centro (mostly from the 2010 El Mayor earthquake).

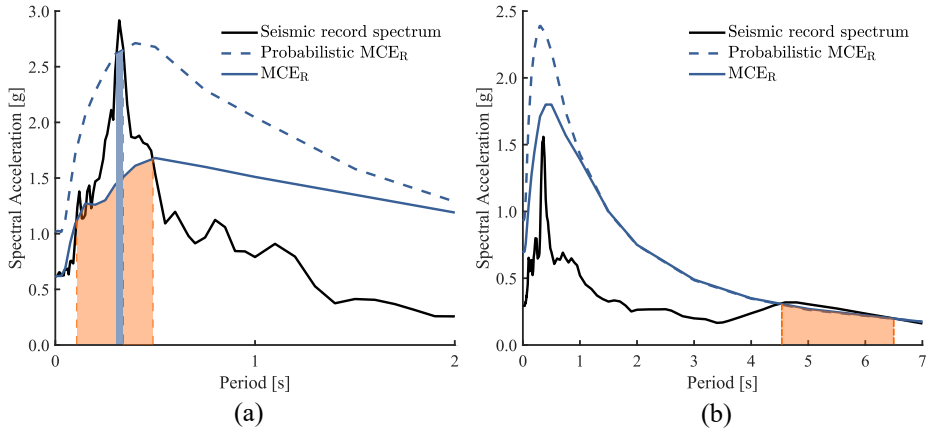

Figure 6. Period-dependent effect of the deterministic cap in the multi-period MCE$_R$ spectrum, exemplified by seismic record spectra from (a) El Centro Array #11 station and (b) Westside Elementary School station during the 2010 El Mayor–Cucapah earthquake. Shaded regions indicate the period range where the recording exceeds the target spectra.

Among the exceedances, 29 recordings are classified as aftershocks based on the $CR_{JB} < 20$ km criterion of Wooddell and Abrahamson (2014), consistent with the Chiou and Youngs (2014) ground–motion model (GMM) used later in our analysis. Of these, nine aftershocks exceed the MCE$_R$, seven the UHS, and five the probabilistic MCE$_R$, all from the 1975 Oroville and 1983 Coalinga sequences. The remaining aftershocks exceed only the DE response spectrum and are mostly associated with the 1983 Coalinga, 1980 Mammoth Lakes, 1994 Northridge, and 1975 Oroville earthquakes. These are all $M < 6$ events, with exceedances mostly below 0.3 s. They could potentially be omitted from the analysis because the reference hazard analysis does not consider aftershock analyses. But we choose to retain them because they still provide information about strong ground shaking, and because the 2024 USGS hazard model (and presumably future codes based on it) do consider aftershocks (Petersen et al., 2024). Further details about aftershock classifications are provided in the Supplemental Material.

Figure 7 reveals that, not surprisingly, regions located in areas affected by the deterministic cap (namely Santa Cruz, Parkfield/Coalinga, and El Centro) exhibit a higher frequency of recordings that exceed the MCE$_R$ spectrum. This trend reflects the effect of the deterministic cap in deflating the design level near faults, consistent with the locations previously observed by Stewart et al. (2020). Importantly, all listed regions contain recordings that exceed the MCE$_R$ and the probabilistic spectra, which is true of most recordings in region 3 (Los Angeles).

Figure 8 shows the range of periods over which recorded spectra exceed their corresponding UHS. For each recording, the period where the highest SA/UHS ratio occurs is designated $T_{\max}$, and used to normalize the horizontal axis plot. The normalized

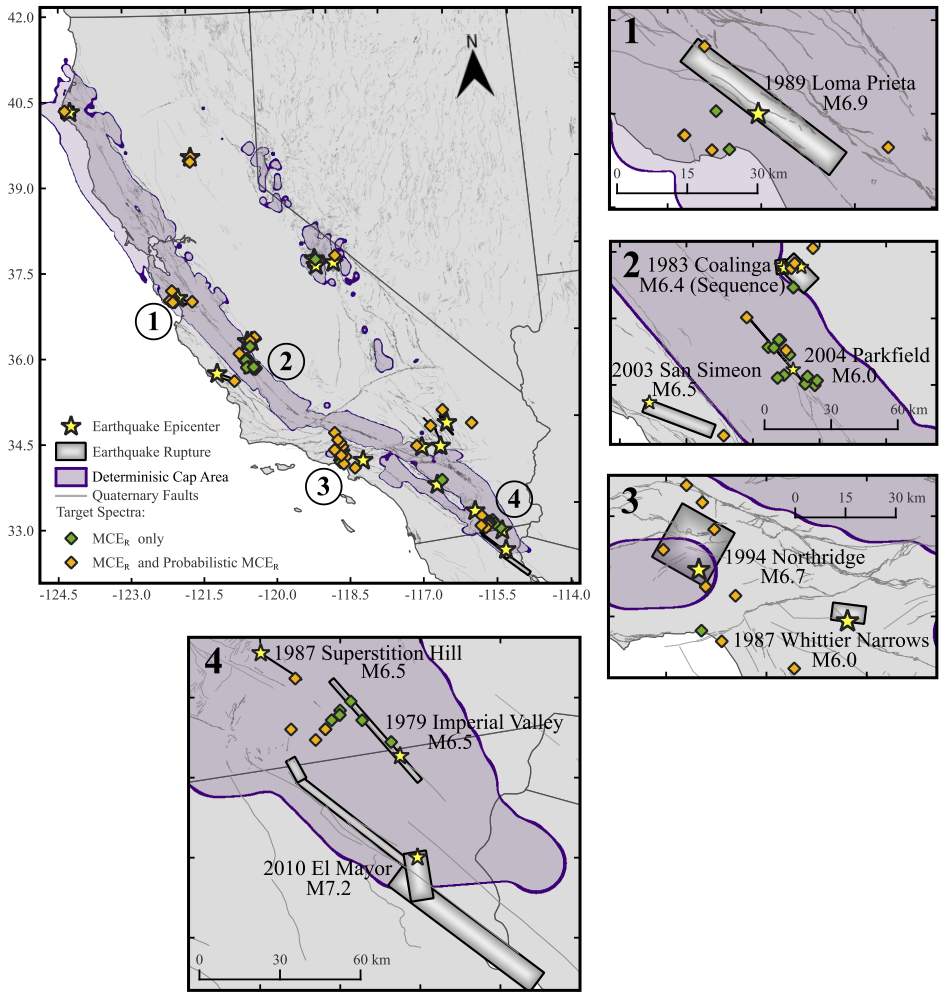

Figure 7. Locations of recording stations with observed exceedances of the MCE$_R$ spectrum or probabilistic MCE$_R$. The shaded region indicates the area affected by the deterministic cap at $T = 1$ s for Site Class CD. Earthquakes causing the exceedances are also shown. Upper left: overview of locations in California. Subpanels: zoomed-in views of selected areas with multiple exceedances.

period range ($T/T_{\max}$) where the median ratio SA/UHS is greater than one (i.e., the recording exceeds the UHS) spans from approximately 0.86 to 1.16. This observation indicates that as the period at which the difference between SA and UHS attains its maximum ($T_{\max}$) increases, the range of periods at which the recorded spectral acceleration exceeds the target spectrum also expands. Thus, although many ground

motions exceed their target spectra at one or more periods, the range of periods with exceedances is often quite narrow.

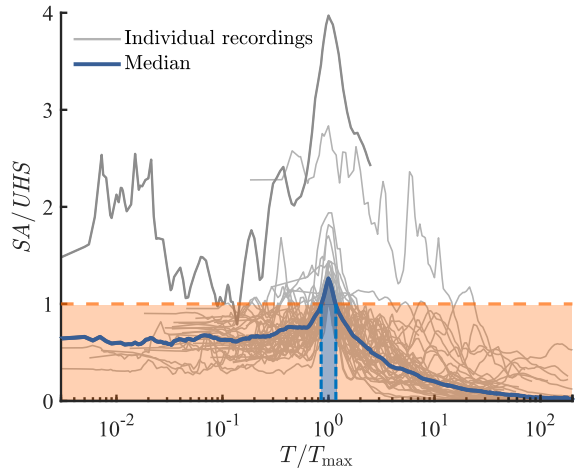

Figure 8. Ratio of spectral acceleration SA to the 2475-year uniform hazard spectrum UHS versus normalized period $T/T_{\max}$ for all recordings that exceed the UHS. Here, $T_{\max}$ is the period at which the ratio between SA and UHS is maximized. The darker grey curve highlights the Lucerne station recording of the M 7.28 1992 Landers earthquake; it is plotted in an alternate style to aid in distinguishing among the highest amplitude spectra in the plot.

Figure 9 compares the magnitude, distance, and ε values of recordings that exceeded the 2475-year return period UHS, to the corresponding disaggregation causal mean parameters (i.e., $\overline{M}$, $\overline{R}_{rup}$, and $\overline{\varepsilon}$). This comparison was made for recordings with exceedances at periods of approximately $T = 0.1$, 1.0, and 5.0 s. In this sense, using a simple exponential filter, we selected the range exceedance periods considered in each reference period: from 0.025 to 0.18 s in $T = 0.1$ s, from 0.49 to 1.51 s in $T = 1.0$ s, from 3.85 to 6.14 s in the $T = 5.0$ s. These comparisons provide insight into the properties of earthquakes that produced exceedances, relative to those predicted by the PSHA calculation that cause exceedances.

The disaggregation and observation metrics are in general agreement, with many points lying close to the diagonal lines on the plots. Looking more precisely, the observed exceedances tend to come from slightly smaller magnitudes, smaller distances, and larger epsilons than the mean disaggregation values. This may be caused in part by the relatively few large-magnitude earthquakes that have occurred in California in recent decades (e.g. Bakun, 1999), leaving more moderate magnitude events ($M < 6.5$) (with close distances and large epsilons to compensate) to cause most of the observed exceedances in the data set.

Figure 9a also shows that exceedances at short periods are generally caused by smaller-magnitude ruptures than exceedances at long periods. This trend is expected due to the more frequent occurrences of small-magnitude events, combined with the

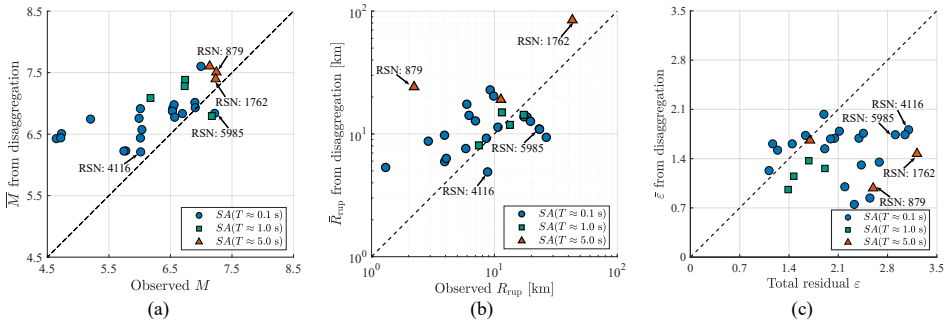

Figure 9. Comparison of observed earthquake parameters at stations where recorded ground motions exceed the UHS for a 2475-year return period and the corresponding disaggregation-based causal mean parameters: (a) observed earthquake magnitude M versus causal mean magnitude $\overline{M}$; (b) observed source-to-site distance R_{rup} versus causal mean distance $\overline{R}_{rup}$; and (c) observed total residual ε versus causal mean epsilon $\overline{\varepsilon}$. All comparisons are shown for events where the observed spectral exceedance periods closely match those selected for disaggregation analysis. Record sequence numbers for selected recordings are annotated to facilitate discussion in the text.

magnitude saturation of short-period response spectra, and is reflected in the similar trend of disaggregation values. This relationship, combined with the dearth of large-magnitude recordings, may also explain why Figure 4a shows more exceedances of the UHS at short periods than long periods. This aligns with the trend that long-period hazard levels are primarily driven by large-magnitude events, which have relatively larger long-period amplitudes, rather than low-to-moderate ones. When a future large-magnitude event occurs in a heavily instrumented part of the study area, we would anticipate seeing a number of recordings that exceed the target spectra at longer periods and, over a longer observational window, an overall increase in exceedances across all periods with a broadly similar proportion of long- to short-period exceedances. Such a pattern of longer-period target spectrum exceedances was seen, for example, in the 2023 large-magnitude events in Turkey (e.g., Gülkan et al., 2023).

Additionally, the total residual shown in Figure 9c can be understood based on how the GMM spectral shape varies with earthquake actual magnitude and source-to-site distance. In this study, the total residual is computed using Chiou and Young's (2014) GMM, which generally produces residuals similar to other GMMs used in the hazard model. Recordings that exceeded the UHS were generally caused by lower-magnitude, nearer earthquake events than the mean disaggregation values, producing lower predicted median spectral accelerations, and higher total residuals when exceedances occurred.

Examples of this trend are RSN 4116 and 5985 (the latter with a larger distance that causes low spectral accelerations) highlighted in Figure 9c; their target spectra along with the GMM spectral acceleration curve are shown in the Supplemental Materials. A similar pattern emerges for long-period exceedances. For instance, RSN 879 exceeds the UHS near $T \approx 5$ s with a total residual more than 2.5 times its mean causal $\overline{\varepsilon}$, even though

its magnitude matches the disaggregation mean and its distance to source R_{rup} is shorter than the disaggregation expectation.

Note that a disagreement between observed metrics and disaggregation means is not evidence of any problem with the PSHA calculation, as many rupture characteristics can produce exceedances, as represented by the full disaggregation distributions rather than the mean, a fact observed in prior studies (Bradley, 2025). An additional long-period exceedance case, along with comparisons between disaggregation parameters and recordings that exceed the MCE_{R} spectrum, are included in the Supplemental Materials.

Discussion

Several justifications for deterministic caps on design spectra have been provided in prior literature. Some have claimed that the use of a deterministic 84th percentile ground motion target spectrum "encompasses the variability in the data by covering it with a maximum credible earthquake" (Krinitzsky, 2002). The frequent exceedances of deterministically capped 84th percentile spectra reported here clearly refute that argument. Further, most of the UHS exceedances were associated with $>$ 84th percentile motions (i.e., motions with $\varepsilon > 1$), as seen in Figure 9c. More sober authors associated with U.S. code development were largely motivated by pragmatic considerations (Stewart et al., 2020). Nevertheless, these deterministic limits can introduce conceptual inconsistencies and elevate collapse risk for structures near active fault zones (e.g. Stewart et al., 2020; Bradley, 2025).

While many ground motions were observed to exceed the considered target spectra at one or more periods, it is much rarer to have them exceed the spectrum over a large range of periods, as shown in Figure 8. While earthquake engineers should certainly consider the possibility that their systems may experience shaking larger than these target spectra at a single period, it is much more unusual for a ground motion to exceed the spectrum at a range of periods. This phenomenon is the motivation for ASCE 7 allowing the use of Conditional Mean Spectra as the target for design and analysis (Haselton et al., 2017).

Given the comparison here of observations to spectral values obtained from hazard analysis, it is natural to wonder whether these results provide insights about whether the underlying hazard analysis is correct (i.e., predicts exceedance rates consistent with what was observed). However, because we do not have information about the periods of time for which each recording station has been operating, we do not have empirical occurrence rates for the observations that could be compared with the hazard predictions. However, the observed earthquakes and ground motions considered here are the same motions used to calibrate the source models and ground motion models used in the underlying hazard studies, so a general internal consistency between the two spectra is expected. Regardless of hazard validation, it is hopefully clear to the reader that exceedances of these "rare" spectra are somewhat plentiful if we look over enough geographic locations and spectral periods.

Conclusions

This study compared 15,111 ground motion recordings from the NGA-West2 database with four corresponding target spectra from ASCE/SEI 7–22 and the 2023 USGS National Seismic Hazard Model. The first three considered target spectra were the maximum considered earthquake (MCE_R), the "probabilistic MCE_R" without a deterministic cap applied, and the design earthquake (DE), all from ASCE/SEI 7–22. Additionally, the 2475-year uniform-hazard spectrum (UHS) from the 2023 USGS National Seismic Hazard Model was considered. We identified exceedances of these target spectra across different periods and interpreted them in light of deterministic capping and probabilistic seismic hazard analysis (PSHA) disaggregation.

Across 105 periods and 1706 stations, we identified 63 recordings that exceeded the risk-targeted MCE_R, 34 that exceeded the probabilistic MCE_R, and 42 that exceeded the UHS. The DE spectrum, defined as two-thirds of MCE_R, was exceeded most often (170 times), as expected. Near major active faults, the ASCE 7-22 deterministic cap reduces MCE_R response spectrum ordinates, especially at short periods, thereby increasing the number of recordings that exceed this target spectrum but not the underlying probabilistic spectrum. This trend is consistent with the regional patterns reported by Stewart et al. (2020).

Regardless of the target spectrum, exceedances were more frequent at short spectral acceleration periods ($T < 1$ s), where low-to-moderate magnitude events predominate and, thus, are more likely to produce large short-period spectral acceleration amplitudes (albeit with low probability in any given ground motion). At longer periods ($T > 1$ s), exceedances are mainly driven by high-magnitude events ($M > 7$). Consequently, exceedances in this period range are sparse because these events are comparatively infrequent in the considered observational set. Nevertheless, when such events occur, they can surpass the target spectra over a broad period range. Future studies following large-magnitude earthquakes will be helpful in evaluating whether the less frequent exceedances of long-period target spectra observed here are due to peculiarities of the considered ground motion data, or indicate some more systematic trend.

Recordings that exceeded the UHS generally involved smaller magnitudes and shorter source–to–site distances than the causal means obtained from PSHA disaggregation. Consequently, total residuals, computed using the Chiou and Youngs (2014) model, were often higher than the mean disaggregation values ε for both short and long periods. However, this finding does not imply a discrepancy with the NSHM; instead, this may be explained by the inherent difference when comparing the mean disaggregation values (aggregating a set of potential earthquake scenarios) with the intensities of individual earthquake recordings.

Overall, these observations highlight that ground-motion exceedances of target spectra based on the 2% probability in 50 years seismic hazard level and 1% risk of collapse in 50 years are both plausible in real earthquake recordings. Forthcoming ASCE 7 editions and other standards that contemplate using deterministic caps or higher risk-target levels must weigh the associated economic and safety implications in light of the observed exceedance cases. Continuing the debate about hazard and risk targets associated with

building code spectra is healthy. However, the debate should be about tradeoffs between costs and safety and not about whether these high-amplitude spectra are realistic. They have been observed many times in the past, and will certainly be observed in the future.

Data and Resources

The code and data that result from this study are openly available in a Github repository in `https://github.com/vhcalderon1/exceeding_design_spectra`. The NGA-West2 recordings database and flatfiles were downloaded from `https://ngawest2.berkeley.edu/`. The ASCE 7-22 DE and MCE_R response spectra were obtained from the ASCE Hazard Tool `https://ascehazardtool.org/`. The UHS spectra and disaggregation data were obtained from the USGS Earthquake Hazard Toolbox (Clayton and Powers, 2023). The Quaternary faults map shown in Figure 7 was obtained from the USGS Faults Database `https://www.usgs.gov/programs/earthquake-hazards/faults` and UNAM Mexico Quaternary Fault Database `https://desarrollo.terradigitalis.unam.mx/maps/681`.

Acknowledgments

Thank you to Nathan Girmay for helpful feedback on our analysis.

Authors' note

This research was conducted while Victor Calderon was at the Department of Civil and Environmental Engineering at Stanford University. He is now at Princeton University and may be contacted at vhcalderon@princeton.edu.

Declaration of conflicting interests

The author(s) declared no potential conflicts of interest with respect to the research, authorship, and/or publication of this article.

Funding

This work was supported in part by the Stanford Urban Resilience Initiative.

Supplemental material

Supplemental material for this article is available online.

ORCID iDs

Victor H. Calderon `https://orcid.org/0009-0004-4666-8871`
Jack W. Baker `https://orcid.org/0000-0003-2744-9599`

References

Ancheta TD, Darragh RB, Stewart JP, Seyhan E, Silva WJ, Chiou BSJ, Wooddell KE, Graves RW, Kottke AR, Boore DM, Kishida T and Donahue JL (2014) NGA-West2 Database. *Earthquake Spectra* 30(3): 989–1005. DOI:10.1193/070913EQS197M. URL https://journals.sagepub.com/doi/10.1193/070913EQS197M.

ASCE (2021) Minimum Design Loads and Associated Criteria for Buildings and Other Structures. DOI:10.1061/9780784415788.

Baker JW, Bradley BA and Stafford PJ (2021) *Seismic Hazard and Risk Analysis*. Cambridge, England: Cambridge University Press. ISBN 978-1-108-42505-6.

Bakun WH (1999) Seismic activity of the San Francisco Bay region. *Bulletin of the Seismological Society of America* 89(3): 764–784. DOI:10.1785/BSSA0890030764.

Bazzurro P and Cornell CA (1999) Disaggregation of seismic hazard. *Bulletin of the Seismological Society of America* 89(2): 501–520. DOI:10.1785/BSSA0890020501.

Beauval C, Bard PY, Hainzl S and Gueguen P (2008) Can Strong-Motion Observations be Used to Constrain Probabilistic Seismic-Hazard Estimates? *Bulletin of the Seismological Society of America* 98(2): 509–520. DOI:10.1785/0120070006. April 1, 2008.

Bommer JJ and Abrahamson NA (2006) Why Do Modern Probabilistic Seismic-Hazard Analyses Often Lead to Increased Hazard Estimates? *Bulletin of the Seismological Society of America* 96(6): 1967–1977. DOI:10.1785/0120060043. URL https://pubs.geoscienceworld.org/bssa/article/96/6/1967-1977/146678.

Bradley BA (2025) Seismic hazard with deterministic maximum limits: Considerations in a New Zealand-specific context. *Bulletin of the New Zealand Society for Earthquake Engineering* 58(1): 1–10. DOI:10.5459/bnzsee.1706. URL https://bulletin.nzsee.org.nz/index.php/bnzsee/article/view/1706.

Brooks EM, Stein S, Spencer BD, Salditch L, Petersen MD and McNamara DE (2018) Assessing Earthquake Hazard Map Performance for Natural and Induced Seismicity in the Central and Eastern United States. *Seismological Research Letters* 89(1): 118–126. DOI:10.1785/0220170124.

Brune J (1996) Precariously balanced rocks and ground-motion maps for southern California. *Bulletin of the Seismological Society of America* 86(1A): 43–54.

Chiou BSJ and Youngs RR (2014) Update of the Chiou and Youngs NGA Model for the Average Horizontal Component of Peak Ground Motion and Response Spectra. *Earthquake Spectra* 30(3): 1117–1153. DOI:10.1193/072813EQS219M. URL https://journals.sagepub.com/doi/10.1193/072813EQS219M.

Clayton BS and Powers PM (2023) USGS Earthquake Hazard Toolbox. DOI:10.5066/P9UAIISF.

Douglas J, Crowley H, Silva V, Marzocchi W, Danciu L and Pinho R (2024) Methods for evaluating the significance and importance of differences amongst probabilistic seismic hazard results for engineering and risk analyses: a review and insights. *Bulletin of Earthquake Engineering* 22(6): 2769–2796. DOI:10.1007/s10518-024-01896-y. URL https://link.springer.com/10.1007/s10518-024-01896-y.

Gerstenberger MC, Marzocchi W, Allen T, Pagani M, Adams J, Danciu L, Field EH, Fujiwara H, Luco N, Ma K, Meletti C and Petersen MD (2020) Probabilistic Seismic Hazard Analysis at Regional and National Scales: State of the Art and Future Challenges. *Reviews of Geophysics* 58(2): e2019RG000653. DOI:10.1029/2019RG000653. URL https://agupubs.onlinelibrary.wiley.com/doi/10.1029/2019RG000653.

Gülkan HP, Akansel VH and Kalkan E (2023) Response spectrum shapes implied by earthquakes in Turkey: Comparisons with design spectra. *Journal of Seismology* 27(4): 681–692. DOI:10.1007/s10950-023-10155-7.

Hamburger R, Pekelnicky R and Furr J (2017) Project 17 Technical Background. In: *Proceedings of the Project 17 Workshop on Seismic Hazard Mapping*. San Francisco, CA, pp. 15–36.

Haselton CB, Baker JW, Stewart JP, Whittaker AS, Luco N, Fry A, Hamburger RO, Zimmerman RB, Hooper JD, Charney FA and Pekelnicky RG (2017) Response History Analysis for the Design of New Buildings in the NEHRP Provisions and ASCE/SEI 7 Standard: Part I - Overview and Specification of Ground Motions. *Earthquake Spectra* 33(2): 373–395. DOI:10.1193/032114EQS039M.

Iervolino I (2022) Ground-Motion Observations and Probabilistic Seismic Hazard: Frequently Asked Questions. *Seismological Research Letters* 93(4): 2360–2366. DOI:10.1785/0220210321. URL https://pubs.geoscienceworld.org/srl/article/93/4/2360/614108/Ground-Motion-Observations-and-Probabilistic.

Iervolino I, Giorgio M and Cito P (2019) Which Earthquakes are Expected to Exceed the Design Spectra? *Earthquake Spectra* 35(3): 1465–1483. DOI:10.1193/032318EQS066O. URL https://journals.sagepub.com/doi/10.1193/032318EQS066O.

Kaneko Y and Goto H (2022) The Origin of Large, Long-Period Near-Fault Ground Velocities During Surface-Breaking Strike-Slip Earthquakes. *Geophysical Research Letters* 49(10): e2022GL098029. DOI:10.1029/2022GL098029. URL https://agupubs.onlinelibrary.wiley.com/doi/10.1029/2022GL098029.

Krinitzsky EL (2002) How to obtain earthquake ground motions for engineering designs. *Engineering Geology* 65(1): 1–16.

Lahr KM, Lahr JC, Lindh A, Bufe CG and Lester FW (1976) The August 1975 Oroville earthquakes. *Bulletin of the Seismological Society of America* 66(4): 1085–1099. DOI:10.1785/BSSA0660041085. URL https://pubs.geoscienceworld.org/bssa/article/66/4/1085/101818/The-August-1975-Oroville-earthquakes.

Luco N, Ellingwood BR, Hamburger RO, Hooper JD, Kimball JK and Kircher CA (2007) Risk-targeted versus current seismic design maps for the conterminous United States. In: *Proceedings of the 2007 Structural Engineers Association of California (SEAOC) Convention*. p. 13p.

Luco N, Rezaeian S, Rukstales KS, Shumway AM, Martinez EM and Smoczyk GM (2021) Gridded earthquake ground motions for the 2020 NEHRP Recommended Seismic Provisions and 2022 ASCE/SEI 7 Standard. DOI:110.5066/P9I0R4O6.

Mak S and Schorlemmer D (2016) A Comparison between the Forecast by the United States National Seismic Hazard Maps with Recent Ground-Motion Records. *Bulletin of the Seismological Society of America* 106(4): 1817–1831. DOI:10.1785/0120150323. URL https://pubs.geoscienceworld.org/bssa/article/106/4/1817-1831/350850.

Minson SE, Baltay AS, Cochran ES, McBride SK and Milner KR (2021) Shaking is Almost Always a Surprise: The Earthquakes That Produce Significant Ground Motion. *Seismological Research Letters* 92(1): 460–468. DOI:10.1785/0220200165. URL https://pubs.geoscienceworld.org/ssa/srl/article/92/1/460/592408/Shaking-is-Almost-Always-a-Surprise-The.

Petersen MD, Shumway AM, Powers PM, Field EH, Moschetti MP, Jaiswal KS, Milner KR, Rezaeian S, Frankel AD, Llenos AL, Michael AJ, Altekruse JM, Ahdi SK, Withers KB, Mueller CS, Zeng Y, Chase RE, Salditch LM, Luco N, Rukstales KS, Herrick JA, Girot DL, Aagaard BT, Bender AM, Blanpied ML, Briggs RW, Boyd OS, Clayton BS, DuRoss CB, Evans EL, Haeussler PJ, Hatem AE, Haynie KL, Hearn EH, Johnson KM, Kortum ZA, Kwong NS, Makdisi AJ, Mason HB, McNamara DE, McPhillips DF, Okubo PG, Page MT, Pollitz FF, Rubinstein JL, Shaw BE, Shen ZK, Shiro BR, Smith JA, Stephenson WJ, Thompson EM, Thompson Jobe JA, Wirth EA and Witter RC (2024) The 2023 US 50-State National Seismic Hazard Model: Overview and implications. *Earthquake Spectra* 40(1): 5–88. DOI:10.1177/87552930231215428.

Petersen MD, Shumway AM, Powers PM, Mueller CS, Moschetti MP, Frankel AD, Rezaeian S, McNamara DE, Luco N, Boyd OS, Rukstales KS, Jaiswal KS, Thompson EM, Hoover SM, Clayton BS, Field EH and Zeng Y (2021) The 2018 update of the US National Seismic Hazard Model: Where, why, and how much probabilistic

ground motion maps changed. *Earthquake Spectra* 37(2): 959–987. DOI:10.1177/8755293020988016. URL https://journals.sagepub.com/doi/10.1177/8755293020988016.

Salditch L, Gallahue MM, Stein S, Neely JS, Abrahamson N and Hough SE (2024) Why do seismic hazard models worldwide appear to overpredict historical intensity observations? *Science Advances* 10(18): eadj9291. DOI:10.1126/sciadv.adj9291.

Stewart JP, Luco N, Hooper JD and Crouse CB (2020) Risk-targeted alternatives to deterministic ground motion caps in U.S. seismic provisions. *Earthquake Spectra* 36(2): 904–923. DOI:10.1177/8755293019892010.

Stirling M and Petersen M (2006) Comparison of the Historical Record of Earthquake Hazard with Seismic- Hazard Models for New Zealand and the Continental United States. *Bulletin of the Seismological Society of America* 96(6): 1978–1994. DOI:10.1785/0120050176.

Wooddell KE and Abrahamson NA (2014) Classification of Main Shocks and Aftershocks in the NGA-West2 Database. *Earthquake Spectra* 30(3): 1257–1267. DOI:10.1193/071913EQS208M. URL https://journals.sagepub.com/doi/10.1193/071913EQS208M.

Zoback MD and Wentworth CM (1989) Structure of the Coalinga area and thrust origin of the earthquake. *United States Geological Survey, Professional Paper; (USA)* 1487. URL https://www.osti.gov/biblio/5542486.

Supplemental Materials

The two-period spectral response acceleration is constructed using site-specific parameters (in this case, S_{MS} and S_{M1}) developed based on the multi-period response spectrum following Section 21.4 and the formulas in Section 11.4.5 of the ASCE 7-22 (ASCE, 2021). A comparison between the two-period target spectra and an example recording is shown in Figure A.1.

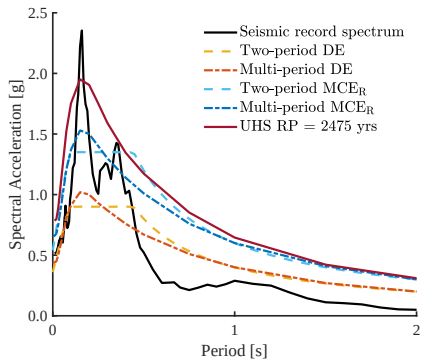

Figure A.1. Comparison of the UCSC Lick Observatory recording spectrum from the 1989 Loma Prieta earthquake with the target spectra at the recording location.

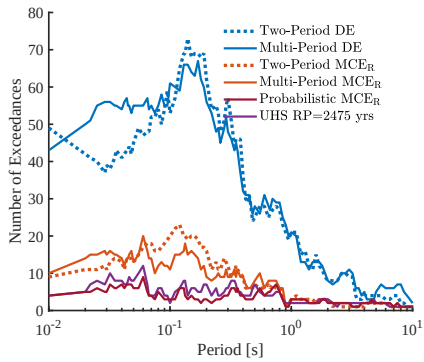

Figure A.2. Number of records that exceeded the target spectra at a given period.

Figure A.2 shows that the two-period and multi-period spectra exhibit comparable exceedance counts, except for periods below 0.1 s. This discrepancy arises due to differences in spectral shapes at short periods, with the two-period spectrum incorporating a constant acceleration platform, as can be seen in Figure A.1. In addition, Figure A.2 reveals that most exceedances occur in all cases at shorter periods than 1.0 s.

A small subset of exceedances arises from aftershocks, identified using the $CR_{JB} <$ 20 km criterion of Wooddell and Abrahamson (2014). Most are associated with the 1975 Oroville and 1983 Coalinga sequences. The Oroville exceedances stem from a single aftershock, potentially linked to denser post–mainshock instrumentation and reservoir-induced stress changes (Lahr et al., 1976). In contrast, the Coalinga exceedances are produced by multiple aftershocks tied to the region's complex faulting behavior (Zoback and Wentworth, 1989).

A comparison between observed earthquake parameters at stations where the MCE_R response spectrum is exceeded and the corresponding disaggregation-based causal mean parameters for a 2,475-year return period is shown in Figure A.3. Compared to Figure 9, Figure A.3 shows a greater number of exceedances at short periods of vibration. Moreover, lower spectral accelerations of the MCE_R at short periods due to the deterministic cap cause lower total residuals ε. Some individual recordings are highlighted as they might be of interest to the reader; however, due to space constraints, their spectral acceleration curves are not plotted herein.

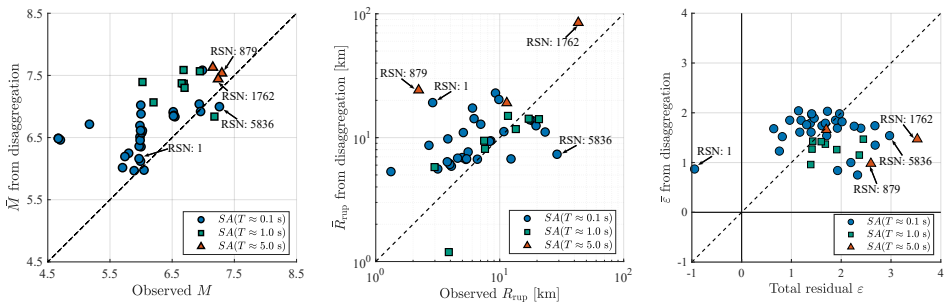

Figure A.3. Comparison of observed earthquake parameters at stations where recorded ground motions exceed the MCE_R response spectrum and the corresponding 2475-years seismic hazard disaggregation-based causal mean parameters: (a) observed earthquake magnitude M versus causal mean magnitude $\overline{M}$; (b) observed source-to-site distance R_{rup} versus causal mean distance $\overline{R}_{rup}$; and (c) observed total residual ε versus causal mean epsilon $\overline{\varepsilon}$. All comparisons are shown for events where the observed spectral exceedance periods closely match those selected for disaggregation analysis. Record sequence numbers for selected recordings are annotated to facilitate discussion in the text.

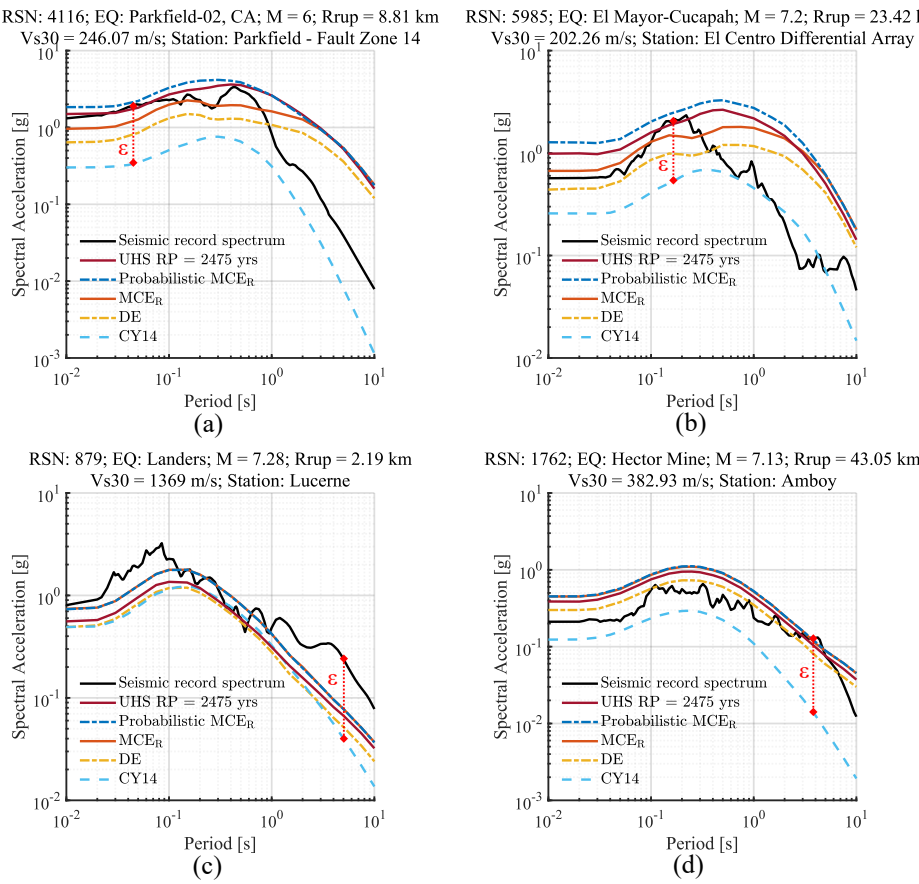

Figure A.4. Sample of recorded ground motions that exceed the UHS. The period and spectral acceleration difference at which the maximum total residual ε occurs are noted.